Hindawi
International Journal of Antennas and Propagation
Volume 2022, Article ID 3339240, 9 pages
https://doi.org/10.1155/2022/3339240

Research Article

A Triple-Band Microstrip Antenna with a Monopole Impedance Converter for WLAN and 5G Applications

Huawei Zhuang,[1] **Fei Li**,[1] **Wei Ding**,[1] **Honghao Tan**,[1] **Junjie Zhuang**,[1] **Changyong Liu**,[1] **Changbin Tian**,[1] **Shiquan Wang**,[2] **Fanmin Kong**,[2] **and Kang Li**[2]

[1]*Shandong Jianzhu University, School of Information & Electrical Engineering, Jinan 250101, China*
[2]*Shandong University, School of Information Science and Engineering, Tsingtao 266237, China*

Correspondence should be addressed to Huawei Zhuang; zhuanghuawei@sdjzu.edu.cn

Received 26 December 2021; Revised 26 February 2022; Accepted 15 March 2022; Published 5 April 2022

Academic Editor: Eng Hock Lim

In this study, a triple-band microstrip antenna with compact size and simple structure is proposed for WLAN and 5G applications. The radiating element consists of a circular patch, a Y-shaped patch, and a monopole impedance converter. In order to obtain the desired operating bands, the monopole impedance converter is inserted between the circular patch and Y-shaped patch. The proposed antenna can work in the frequency range of 2.38~2.53 GHz, 3.29~4.11 GHz, and 4.72~5.01 GHz, with the corresponding peak gains of 4.09 dBi (2.4 GHz), 2.95 dBi (3.5 GHz), and 4.01 dBi (4.9 GHz), respectively. The measures' results are in approximate agreement with the simulated values, which shows that the proposed compact antenna can offer omnidirectional radiation, appropriate gains, and sufficient bandwidths.

1. Introduction

In recent years, enhanced vehicle-to-everything, Internet of things, etc., need better data ability with high speed transmission, rapid response, and stable reliability [1]. To meet the above demands, the network technology is being shifted towards the fifth generation (5G), which aims to provide ultra-fast peak data rate, small mobility interruption time, and high transmission reliability [2]. As a terminal of global mobile data traffic, various antennas have been proposed and designed for 5G and other applications. Of all the antenna structures, microstrip antenna has some significant advantages and characteristics such as low profile, easy fabrication, mechanical stability, better compatibility, and flexible scalability.

In order to satisfy the 5G and other applications, multiple-input-multiple-output (MIMO) can highly improve the data rate, capacity, and link reliability [3]. By incorporating multiantenna systems at the transmitter as well as the receiver, $m \times n$ MIMO 5G antenna array can achieve high data throughput with good isolation and high efficiency [4–6]. In order to satisfy the low isolation degree requirement, a two-port circularly polarized antenna is designed with a rectangle ring ground plane and two T-shaped radiation patches [7]. In [8], a dual-polarization microstrip 5G MIMO antenna array is proposed with eight microstrip antenna elements arranged on the back cover of a mobile phone. Feeding networks and shorted patches' structure are proposed to realize the broadband dual-polarized filtering antenna [9]. Metamaterial structures are also used to realize the circularly polarized antenna with miniaturized size and high radiation efficiency [10]. A beam-switchable antenna is proposed with a crossover including substrate integrated waveguide and dielectric slab [11]. In addition, the fiber-reinforced plastic materials [12], the solar cells [13], airy beam at microwave frequency [14], and high-order mode in circular patch [15] are also introduced to improve the performance of the antennas.

Due to the complexity of the application environment, the pure 5G antenna cannot satisfy the demands of different users. Thus, it is required to integrate 5G frequency band with other spectrum such as WLAN, LTE, WiMAX, and

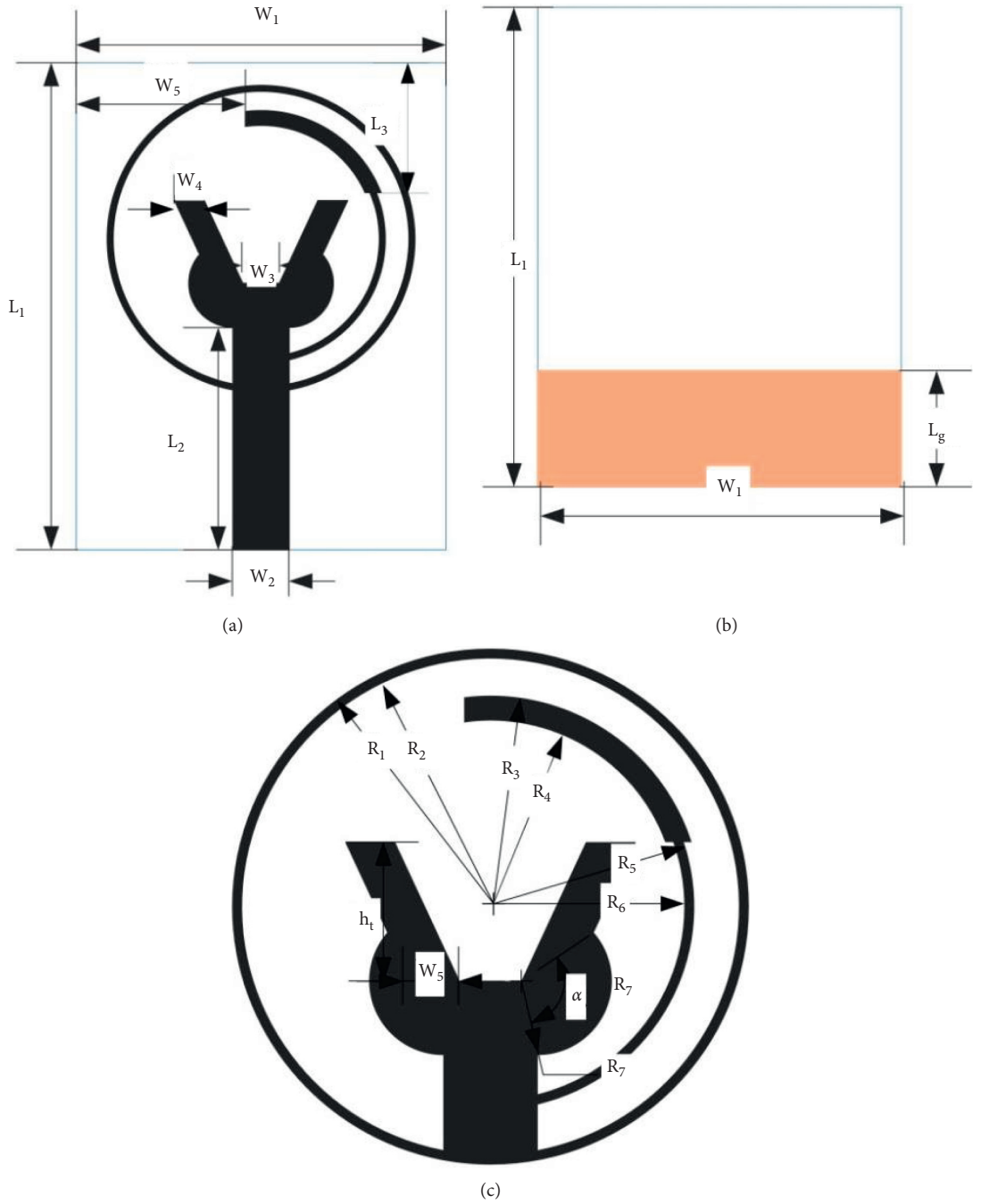

Figure 1: (a) Front view, (b) back view, and (c) radiating element of the proposed antenna.

GPS application. The multiband slotted antenna is formed by a T-shaped feed patch and a rectangular slot on top side of the substrate, which covers the GPS/WiMAX/WLAN bands [16]. A triple-band antenna consisting of a Franklin monopole strip and a rectangular patch is proposed with the operating bands at WLAN, WiMAX, and 5G, respectively [17]. In [18], a dual-band LTE-R and 5G antenna is realized by stacked configuration consisting of a double dielectric substrate, a circular patch, and five elliptical patches. By integrating a stepped patch and a ground plane [19], a low-profile multislot patch antenna is presented for LTE and 5G applications. Usually, the above multiband slot antennas have a larger size to ensure adequate current path on the radiating plane or ground plane. In order to facilitate the integration into the back cover of the handheld devices, a multiband antenna with more compact size and simple structure is desirable for WLAN and 5G application.

In this study, a compact triple-band microstrip antenna is proposed and designed for WLAN and 5G applications. The proposed antenna consists of a circular patch, a Y-shaped patch, and a monopole impedance converter. The realization principle is based on the half-wavelength

Table 1: The detailed dimensions of the proposed antenna.

Parameter	L_1	L_2	L_3	W_1	W_2	W_3	W_4	W_5	W_6
Size (mm)	30	15	8.8	25	3.8	2.5	2	11.4	2.6
Parameter	L_g	h_t	R_1	R_2	R_3	R_4	R_5	R_6	R_7
Size (mm)	8	5.6	10.4	10	8.7	7.7	8.4	8	3
Parameter	α								
Degree (°)	131								

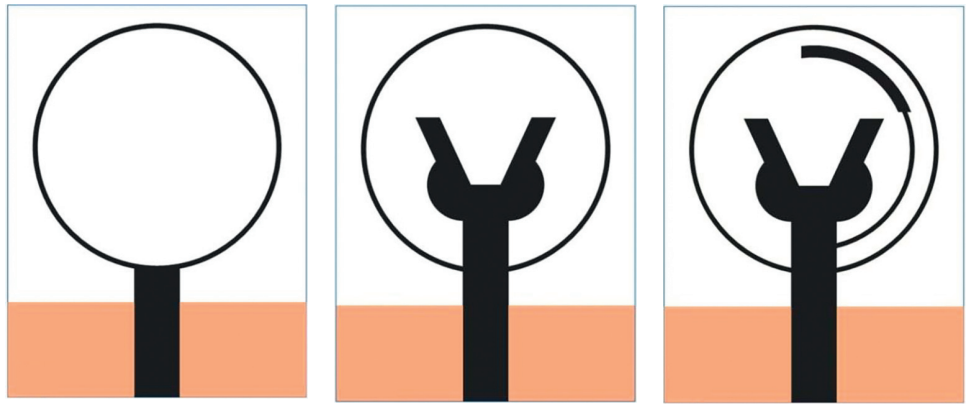

(a) (b) (c)

Figure 2: Design evolution of (a) antenna-1, (b) antenna-2, and (c) antenna-3.

(quarter-wavelength) resonance in the circular patch and the Y-shaped patch structure. The proposed antenna can generate the operating bands of 2.38~2.53 GHz, 3.29~4.11 GHz, and 4.72~5.01 GHz, respectively. A prototype of the antenna is manufactured and measured, and the simulation and measurement results confirm that the triple-band antenna has enough bandwidth to cover the desired WLAN and 5G applications.

2. Antenna Design Process and Parametric Analysis

Figures 1(a)~1(c) illustrate the schematic views of the proposed antenna including the front view, back view, and the radiating element. The radiating element is printed on top of the substrate, consisting of a circular patch, a Y-shape-like strip with two fan-shaped patches and a monopole impedance converter. The feed line with 50-ohm characteristics impedance is etched on the FR4 substrate, and the rectangle ground plane is printed on the backside of the dielectric substrate. In addition, the relative permittivity of the FR4 substrate is set as $\varepsilon_r = 4.4$ with the dielectric loss tangent of $\delta = 0.02$. The proposed antenna is analyzed and optimized using the HFSS Microwave Studio simulator. The detailed parameters of the proposed antenna are listed in Table 1.

Figure 2 displays the design evolution of the proposed antenna, and the corresponding simulated reflection coefficients (S_{11}) are shown in Figure 3. From Figure 2(a), it can be seen that antenna-1 is a simple monopole antenna composed of a circular ring and a rectangular ground plane. As demonstrated in Figure 3, there is only one operating band between 2.40~2.50 GHz centered at 2.45 GHz. In our design evaluation section from antenna-1 to antenna-2, we repeatedly test different kinds of radiating element to obtain another two resonant frequencies. After consulting a lot of relevant references, the Y-shape-like strip with two fan-shaped patch is selected inside the circular patch with a more compact scale. By introducing a Y-shape-like strip with two fan-shaped patches into the circular ring (antenna-2), the antenna can excite the other two operating bands, which can be used in 5G scenes. In order to obtain more compact structure, the Y-shaped monopole patch can be easily bested within the circular monopole patch and the impedance converter, which can be set as the unit cell of the MIMO antennas and easy to integrate in the back cover of the handheld devices. In order to optimize the first and third operating bands to better satisfy the requirements working frequencies, a monopole impedance converter is inserted between the Y-shaped patch and the circumscribed circle patch. It is obviously observed from Figure 3 that the operating bands of antenna-3 are 2.38~2.53 GHz, 3.29~4.11 GHz, and 4.72~5.01 GHz with the center frequencies of 2.4 GHz, 3.5 GHz, and 4.9 GHz, respectively, which satisfy the bandwidth requirements of WLAN and 5G applications.

In our proposed antenna, the realization principle is based on the half-wavelength (quarter-wavelength) resonance in the monopole radiating element with a circular patch or a Y-shaped patch structure. From Figure 3, it can be seen that the antenna-1 is a simple monopole antenna composed of a circular patch, which is fed by a 50 Ω microstrip line. The length of half of the circular patch

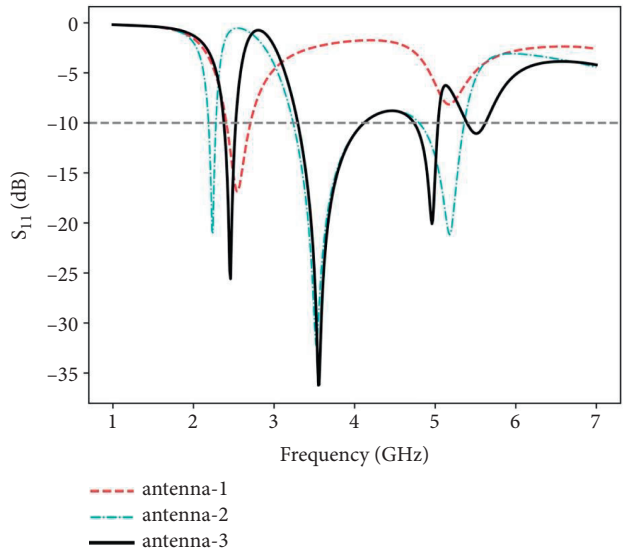

Figure 3: Simulated reflection coefficients S_{11} from antenna-1 to antenna-3.

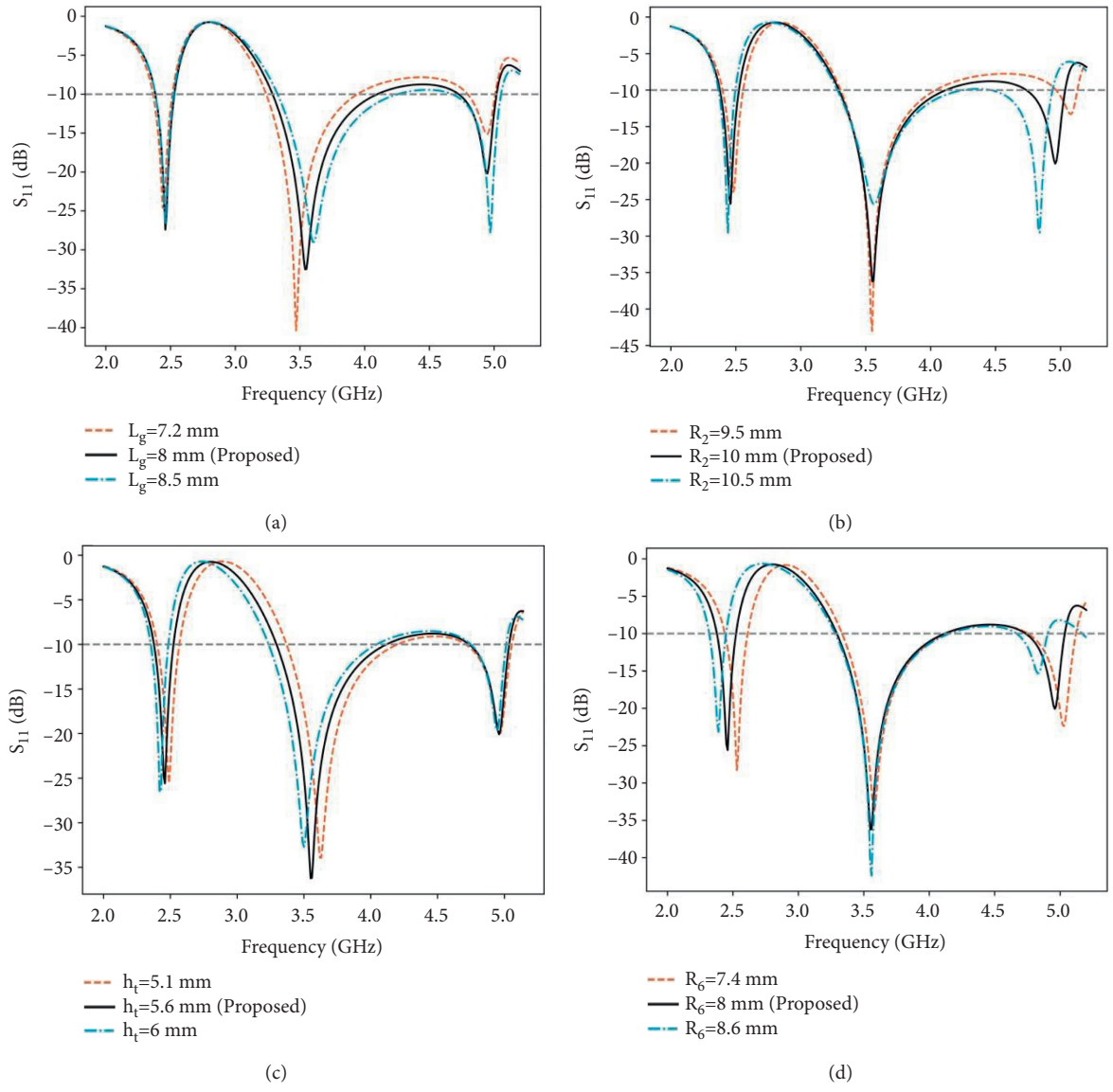

Figure 4: Simulated reflection coefficients S_{11} with different parameter values of (a) L_g, (b) W_2, (c) W_3, and (d) R_6.

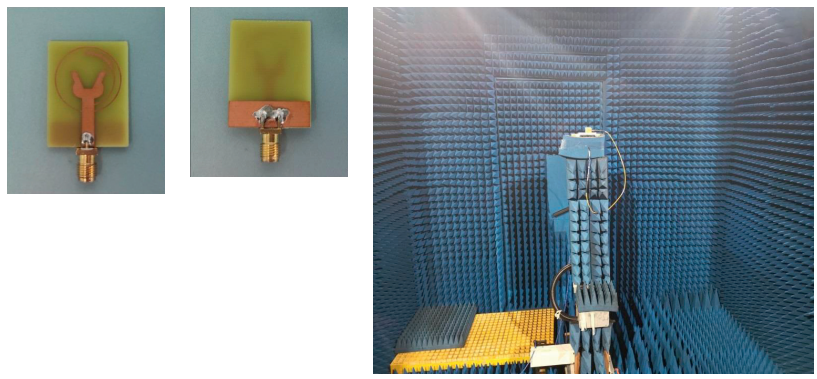

(a) (b) (c)

Figure 5: (a) Front and (b) back views of the fabricated antenna prototype. (c) Photograph of the measurement environment.

$(\pi * r - w_2)$ is optimized to satisfy half-wavelength of the first resonance frequency at 2.45 GHz. The corresponding resonant frequency of antenna-1 is given by

$$f_1 = \frac{c}{2 \times \sqrt{\varepsilon_{\text{eff}}} \times (\pi * r - w_2)}, \quad (1)$$

where $\varepsilon_{\text{eff}} \approx \varepsilon_r + 0.5$ and c is the speed of light. And then, antenna-2 is obtained by introducing a Y-shape-like strip with two fan-shaped patch into the circular ring. By carefully optimizing the structure parameters of the Y-shape-like strip, Antenna-2 can generate another two resonant frequencies working in 5G scenes without increasing the size of the antenna. From Figure 3, it can be found that antenna-2 has two operating bands with the resonant frequencies in the vicinity of 3.5 and 4.9 GHz. The effective length of Y-shape-like strip with two fan-shaped patch should be half (a quarter) of the guided wavelength, which can be approximately calculated by

$$f_m = \frac{c \times m}{4 \times \sqrt{\varepsilon_{eff}} \times \left(L_2 + R_7 + \sqrt{h_t^2 + W_5^2}\right)}, \quad m = 1, 2 \ldots. \quad (2)$$

In order to better analyze the operating principle of the proposed antenna, the variations of different dimensional parameters are investigated. Figure 4(a) demonstrates the variation of the simulated reflection coefficients with L_g It can be observed from the plot that the main operating frequency band of 5G is strongly dependent on the value of L_g. As the value of L_g decreases, the third resonant mode moves towards the second mode, and the bandwidth of the first resonant bandwidth becomes narrower than before. Figure 4(b) presents the simulated reflection coefficients for different values of R_2. As the figure describes, the first and second resonant mode are almost unchanged, and the third frequency demonstrates redshift obviously. From the above analysis, we can see that the desired third band for 4.9 GHz can be tuned by adjusting R_2. As described in Figure 4(c), by increasing the value of ht, the first and second operating bands have an obvious redshift while the third band changed slightly. Thus, the ranges of these two operating bands can be effectively adjusted by changing the value of ht. Figure 4(d) displays the variation of the reflection coefficients for different values of R_6. It can be observed that, with the increase of R_6, the first and third bands show redshift while the middle band keeps unchanged.

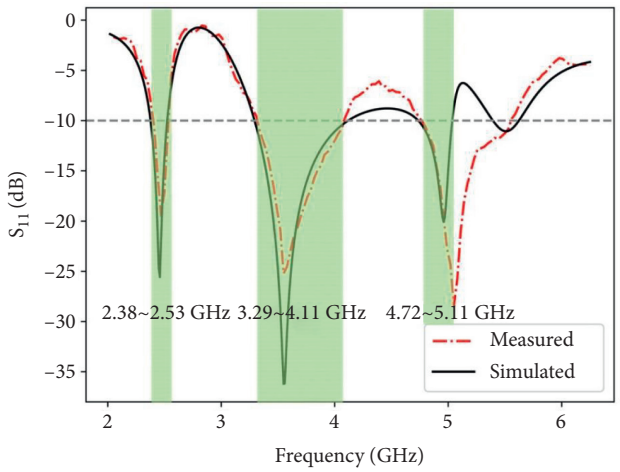

Figure 6: Simulated and measured reflection coefficients S_{11} of the proposed antenna.

3. Results and Discussion

Figures 5(a) and 5(b) show the front and back views of the fabricated antenna prototype. The radiation characteristics of the antenna are measured in the anechoic chamber, and Figure 5(c) shows its actual environment for the far-field measurements. The overall size of the anechoic chamber is 8 m (length) × 6 m (width) × 3.5 m (height). During the measurement process, the distance between the auxiliary horn antenna and the antenna under test is set as 5 m, which can completely satisfy the requirements of far-field measurement. The measured reflection coefficients together with the simulated values are shown in Figure 6, from which we can see that three operating frequency bands of the antenna ($S_{11} \leq 10$ dB) are 2.38~2.53 GHz, 3.29~4.11 GHz, and 4.72~5.01 GHz, respectively. As shown in the plot, the simulated and measured results have an approximate agreement in the working frequency band of the antenna.

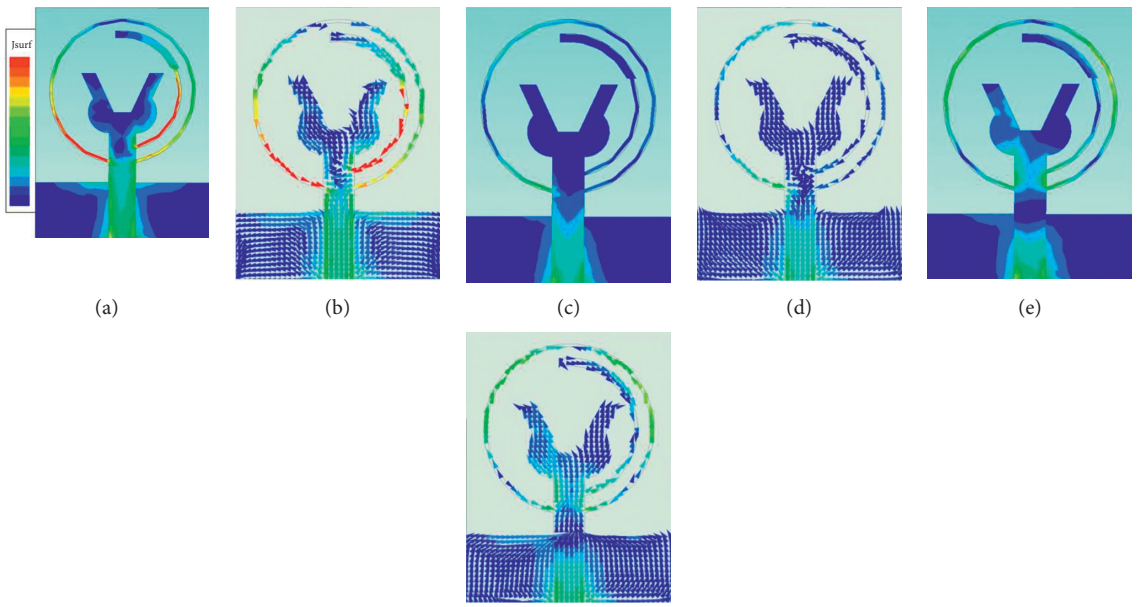

Figure 7: Simulated surface current distributions at (a) 2.4 GHz, (c) 3.5 GHz, and (e) 4.9 GHz, and the corresponding current vector distribution at (b) 2.4 GHz, (d) 3.5 GHz, and (f) 4.9 GHz.

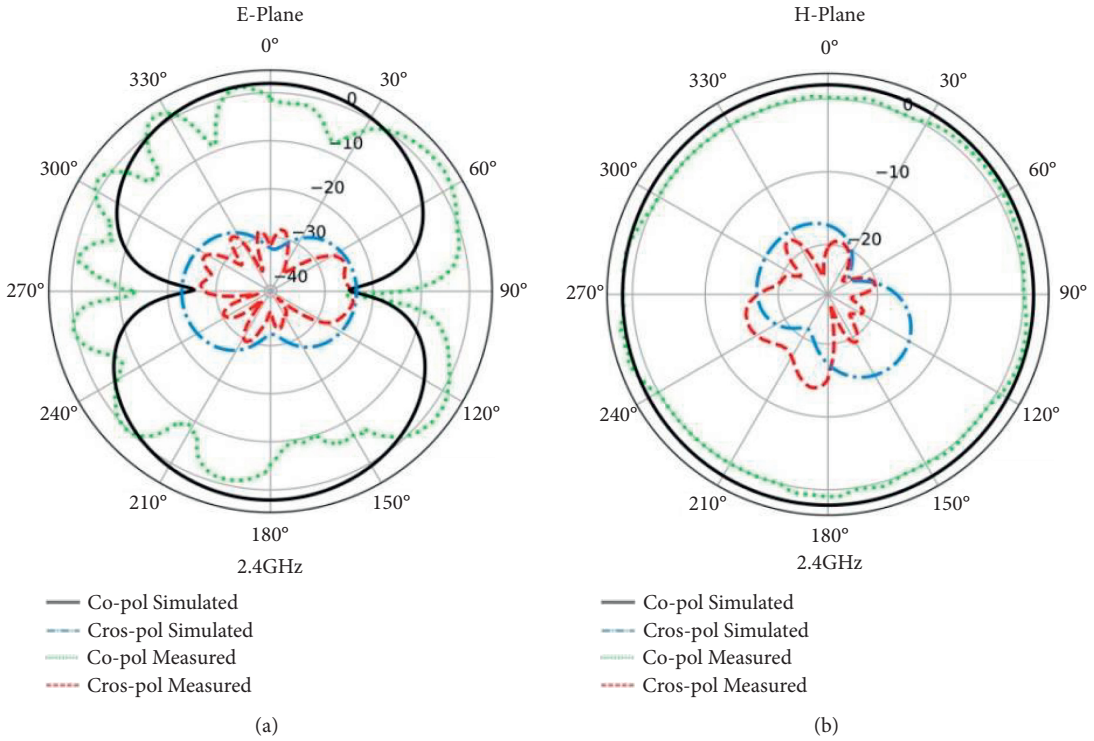

Figure 8: Continued.

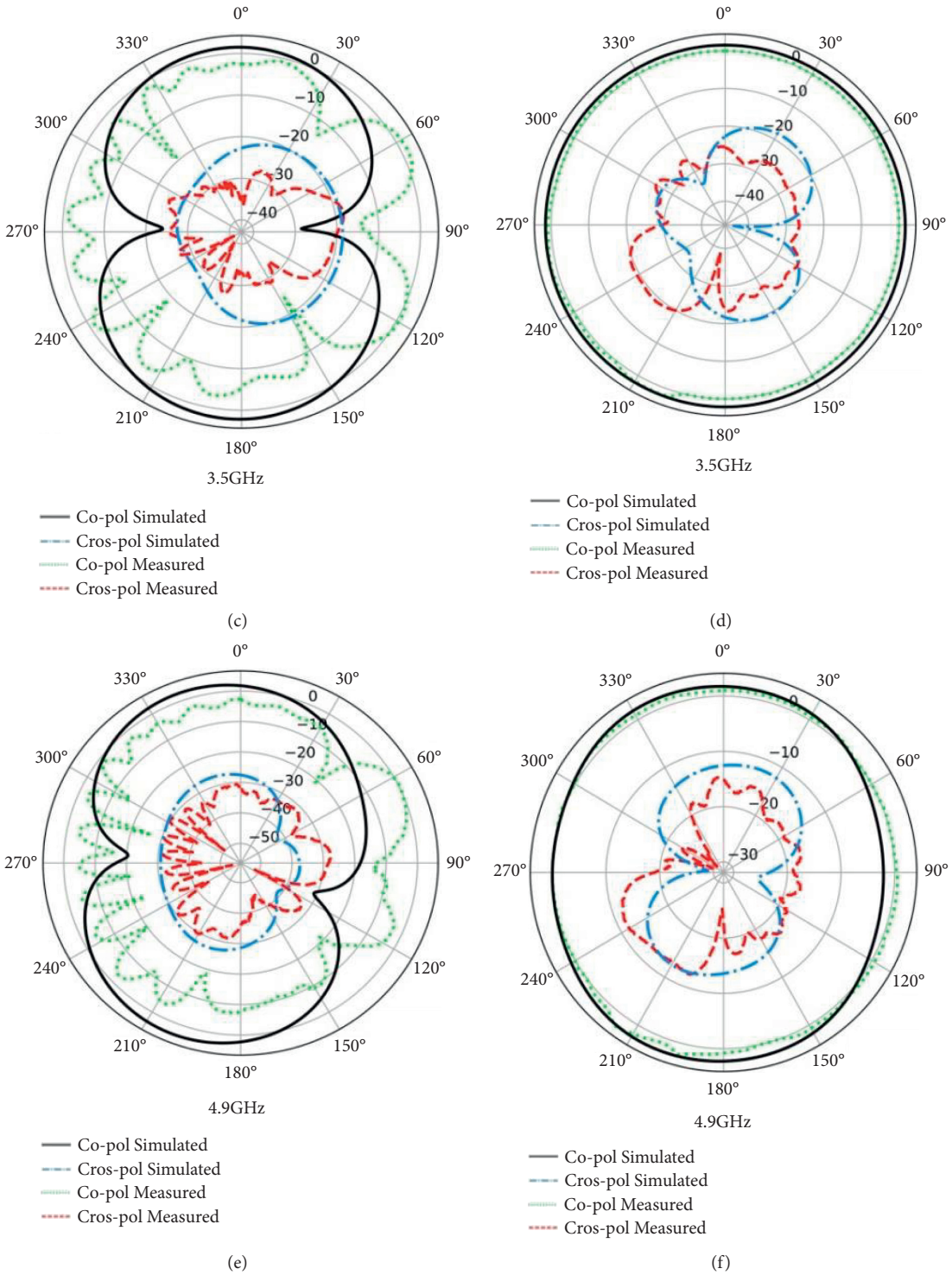

Figure 8: Simulated and measured 2D (a) co-polar and (b) cross-polar radiation patterns.

The discrepancies between the simulated and measured results may be attributed to the fabrication inaccuracy, the abrasion of the patch, and the welding errors of the connector.

To better understand the working mechanism of the proposed antenna, the simulated current and current vector distributions at the resonant frequencies of 2.4 GHz, 3.5 GHz, and 4.9 GHz are shown in Figure 7. From Figures 7(a) and 7(b), it can be seen that the surface current is mainly distributed along the lower part of the circular ring and monopole impedance converter. It is illustrated that the resonant frequency of 2.4 GHz is generated by the combination between the circular ring and the monopole impedance converter. Due to the introduction of the monopole

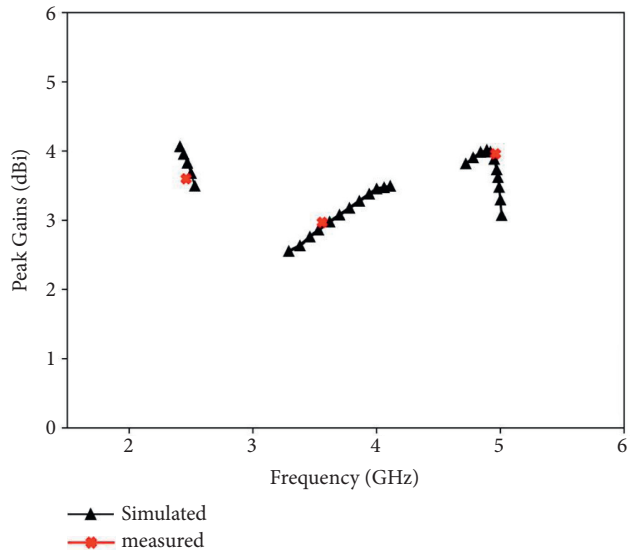

Figure 9: Simulated and measured peak gains at different operating bands.

Table 2: Comparison of the proposed antenna with other previously reported antennas.

Refs.	Operating bands (≤10 dB)	Antenna dimensions (m^3)	Peak gains (dBi)	Profile	Substrate	Applications	Omnidirectional patterns
[4]	3.4–3.8 GHz	75 × 150 × 1.6	3	Planar	FR4	5G	No
[5]	3.3–4.2 GHz	42 × 42 × 1	None	Planar	FR4	5G	No
[6]	3.3–3.6 GHz 4.8–5.0 GHz	150 × 70 × 0.8	None	Planar	FR4	5G	No
[7]	3.3–4.2 GHz	37 × 30 × 0.8	2.5	Planar	FR4	5G	No
[8]	4.37–5.5 GHz	150 × 72 × 1.2	3.7	3D	FR4	5G	No
[9]	3.3–5.1 GHz	60 × 60 × 8	8.1	3D	Rogers RO4003	5G	No
[10]	3.30–3.80 GHz	50 × 50 × 3.5	5.4	3D	F4BK	5G	No
[11]	4.25–5.82 GHz	80 × 80 × 6	9.1	3D	F4BME220	5G	No
[13]	4.8–5 GHz	80 × 80 × 3.76	10.85	3D	F4BM350RUILONG220	5G	No
[18]	0.66–0.79 GHz 3.28–3.78 GHz	180 × 60 × 1.6	2.46.1	3D	FR4	LTE5G	No
Proposed	2.38–2.53 GHz 3.29–4.11 GHz 4.72–5.01 GHz	30 × 25 × 1.59	4.092.214.01	Planar	FR4	WLAN5G	Yes

impedance converter, the distribution of the surface current is not symmetrical along the circular ring. Despite the emergence of the middle band is attributed to the introduction of the Y-shape-like strip with two fan-shaped patches, the current is mainly distributed in the left side of the circular ring, as shown in Figures 7(c) and 7(d). This is because that the currents on the monopole impedance converter and the right side of the circular ring have opposite directions, which causes the radiation energy to be cancelled. At 4.9 GHz, it is found in Figures 7(e) and 7(f) that the current is mainly focused on the circular ring and the Y-shape-like strip.

The simulated and measured 2D co-polar and cross-polar radiation patterns at the frequencies of 2.4 GHz, 3.5 GHz, and 4.9 GHz are shown in Figure 8. It can be observed from the plot that the proposed antenna has a stable omnidirectional radiation pattern. Moreover, the cross-polarized radiation distributions are significantly less than the co-polarized counterparts. The difference between the simulated and measured 2D radiation pattern in E-plane may be caused by fabrication tolerance, chamber scattering, measurement error, etc. Thus, the designed antenna exhibits stable radiation patterns over the operating band, which satisfies the requirement for 5G and other wireless applications.

As shown in Figure 9, the simulated peak gain of the proposed antenna is 3.56~4.16 dBi, 2.45~3.6 dBi, and 3.07~4.01 dBi in 2.38~2.53 GHz, 3.29~4.11 GHz, and 4.72~5.01 GHz, respectively, while the measured values are 3.60 dBi, 2.95 dBi, and 3.96 dBi at 2.4 GHz, 3.5 GHz, and 4.9 GHz, respectively. From Figure 9, it can be found that the gains of the middle band are lower than that of the upper and lower bands. Due to the opposite current vector direction on the monopole impedance converter and the right side of the circular ring at 3.5 GHz, the peak gain is relatively weaker than that at 2.4 GHz or 4.9 GHz. The gain values mainly depend on the current intensity on the radiating element in

the antenna, which converts to the radiating energy of the electromagnetic field. From the simulated surface current distributions in Figure 7, we can see that the current intensity in Figure 7(d) is weaker than any other distribution in Figures 7(b) or 7(f). Table 2 displays the comparison of the performance between proposed and other previously represented antennas. Through the comparison with the references, it can be observed that our proposed antenna can provide enough bandwidths, appropriate gains, and omnidirectional radiation characteristics with more compact size.

4. Conclusions

A triple-band compact microstrip antenna is proposed for WLAN and 5G applications. The radiation element of the proposed antenna consists of a circular ring, a Y-shape-like patch, and a monopole impedance converter. With the help of the monopole impedance converter, the proposed antenna can be optimized in the operating bands of 2.38~2.53 GHz, 3.29~4.11 GHz, and 4.72~5.01 GHz, respectively. From the experimental and measured results, we can see that the antenna has stable omnidirectional patterns, appropriate gains, and enough bandwidth. By comparing the performance with the previously presented antenna, the proposed antenna is a suitable choice to be applied for the 5G antenna design and other wireless applications.

Data Availability

The underlying data supporting the results of your study can be found within the article.

Conflicts of Interest

The authors declare that they have no conflicts of interest.

Acknowledgments

This work was supported by the Natural Science Foundation of Shandong (ZR2021QD066).

References

[1] H. Yu, H. Lee, and H. Jeon, "What is 5G? Emerging 5G mobile services and network requirements," *Sustainability, MDPI*, vol. 9, no. 10, pp. 1–12, 2017.

[2] A. Dogra, R. K. Jha, and S. Jain, "A survey on beyond 5G network with the advent of 6G: architecture and emerging technologies," *IEEE Access*, vol. 9, Article ID 67512, 2021.

[3] Q.-U.-A. Nadeem, A. Kammoun, M. Debbah, and M.-S. Alouini, "Design of 5G full dimension massive MIMO systems," *IEEE Transactions on Communications*, vol. 66, no. 2, pp. 726–740, 2018.

[4] N. O. Parchin, Y. I. A. Al-Yasir, A. H. Ali et al., "Eight-element dual-polarized MIMO slot antenna system for 5G smartphone applications," *IEEE Access*, vol. 7, Article ID 15612, 2019.

[5] I. R. R. Barani, K.-L. Wong, Y.-X. Zhang, and W.-Y. Li, "Low-profile wideband conjoined open-slot antennas fed by grounded coplanar waveguides for $4\times4\,\,5$ G MIMO operation," *IEEE Transactions on Antennas and Propagation*, vol. 68, no. 4, pp. 2646–2657, 2020.

[6] W. Hu, X. Liu, S. Gao et al., "Dual-band ten-element MIMO array based on dual-mode IFAs for 5G terminal applications," *IEEE Access*, vol. 7, Article ID 178476, 2019.

[7] A. K. Dwivedi, A. Sharma, A. K. Pandey, and V. Singh, "Two port circularly polarized MIMO antenna design and investigation for 5G communication systems," *Wireless Personal Communications*, vol. 120, no. 3, pp. 2085–2099, 2021.

[8] B. Cheng and Z. Du, "Dual polarization MIMO antenna for 5G mobile phone applications," *IEEE Transactions on Antennas and Propagation*, vol. 69, no. 7, pp. 4160–4165, 2021.

[9] Y. Zheng and W. Sheng, "Compact dual-polarized filtering antenna with enhanced bandwidth for 5G sub-6 GHz applications," *International Journal of RF and Microwave Computer-Aided Engineering*, vol. 31, no. 9, pp. 1–14, 2021.

[10] Z. Wang, T. Liang, and Y. Dong, "Metamaterial-based , compact, wide beam-width circularly polarized antenna for 5G indoor application," *Microwave and Optical Technology Letters*, vol. 63, no. 8, pp. 2171–2178, 2021.

[11] Y. Cheng and Y. Dong, "Wideband beam-switchable antenna loaded with dielectric slab for 5G applications," *IEEE Antennas and Wireless Propagation Letters*, vol. 20, no. 8, pp. 1557–1561, 2021.

[12] C. M. Preddy, R. Singh, P. H. Aaen, and S. R. P. Silva, "Integrated carbon-fiber-reinforced plastic microstrip patch antennas," *IEEE Antennas and Wireless Propagation Letters*, vol. 19, no. 4, pp. 606–610, 2020.

[13] Y. Luo, J. Lai, N. Yan, W. An, and K. Ma, "Integration of aperture-coupled multipoint feed patch antenna with solar cells operating at dual compressed high-order modes," *IEEE Antennas and Wireless Propagation Letters*, vol. 20, no. 8, pp. 1468–1472, 2021.

[14] Z. Yang, G. Wen, W. Hu, D. Inserra, Y. Huang, and J. Li, "Microwave airy beam generation with microstrip patch antenna array," *IEEE Transactions on Antennas and Propagation*, vol. 69, no. 4, pp. 2290–2301, 2021.

[15] S. Radavaram, S. Naik, and M. Pour, "Stably polarized wideband circular microstrip antenna excited in TM12 mode," *IEEE Transactions on Antennas and Propagation*, vol. 69, no. 4, pp. 2370–2375, 2021.

[16] Y. F. Cao, S. W. Cheung, and T. I. Yuk, "A multiband slot antenna for GPS/WiMAX/WLAN systems," *IEEE Transactions on Antennas and Propagation*, vol. 63, no. 3, pp. 952–958, 2015.

[17] M. E. Yassin, H. A. Mohamed, E. A. F. Abdallah, and H. S. El-Hennawy, "Single-fed 4G/5G multiband 2.4/5.5/28 GHz antenna," *IET Microwaves, Antennas & Propagation*, vol. 13, no. 3, pp. 286–290, 2019.

[18] A. K. Arya, S. J. Kim, and S. Kim, "A dual-band Antenna for lte-R and 5g lower frequency operations," *Progress In Electromagnetics Research Letters*, vol. 88, pp. 113–119, 2020.

[19] R. Azim, A. M. H. Meaze, A. Affandi et al., "A multi-slotted antenna for LTE/5G Sub-6 GHz wireless communication applications," *International Journal of Microwave and Wireless Technologies*, vol. 13, no. 5, pp. 486–496, 2021.